PROCEEDINGS, Thirty-Eighth Workshop on Geothermal Reservoir Engineering
Stanford University, Stanford, California, February 11-13, 2013
SGP-TR-198

MODELING RESERVOIR STIMULATION INDUCED BY WELLBORE FLUID INJECTION

Eyal Shalev and Vladimir Lyakhovsky

Geological Survey of Israel
30 Malkhei Israel
Jerusalem, 95501, Israel
e-mail: eyal@gsi.gov.il

ABSTRACT

A novel numerical software: "*Hydro-PED*", is presented for modeling hydraulic stimulation by wellbore fluid injection. The coupled equations of poro-elastic deformation with damage evolution, and groundwater flow are solved using the Explicit Finite Difference Lagrangian Method for solid deformation and the Finite Element Method for fluid mass conservation. Rock properties are coupled with the state of damage, and seismic events are nucleated as damage grows to a value (~1) that causes the loss of convexity of the elastic strain energy function. The seismic event is simulated by a stress drop using the Drucker-Prager model and produces a rapid release of the elastic energy and accumulation of a permanent plastic strain. Elastic and hydrological properties are coupled with the damage of the rock and as a result may vary by nine orders of magnitude as the rock is damaged and healed. This numerical implementation takes advantage of the ability of the explicit scheme to account for large variations in the stiffness values in neighboring elements with no numerical instabilities.

Results show that the propagation of the enhanced damaged reservoirs could be divided into three stages. 1) Fluid flow into the rock with no seismic events. 2) Seismic events begin and accelerate. Pore pressure at the tip of the reservoirs is above 90% of the pressure in the injection well. The velocity of the advancing reservoirs is limited only by the rate of damage accumulation. 3) Reservoir growth decelerate (>30 hours). Fluid transport becomes a limiting factor as the reservoirs are too long to efficiently transfer the pressure from the well to the reservoir tip.

INTRODUCTION

Hydraulic stimulation by wellbore fluid injection is widely used to increase permeability in hydrocarbon and geothermal reservoirs (Pearson, 1981; Zoback and Harjes, 1997; Cuenot et al., 2008; Fischer et al., 2008; Šílený et al., 2009). However, only a few studies have attempted to model the entire process, probably because of its complexity (Tang et al., 2002; Adachi et al., 2007; Kohl and Megel, 2007; Hossain, and Rahman, 2008; Wang et al., 2009; Baisch et al., 2010; Lee and Ghassemi, 2011; Zhao and Young, 2011). The processes associated with hydraulic stimulation include: fluid flow, deformation and brittle failure of the porous media, and generation of seismic events resulting with stress drop. The model should account for dependency of the mechanical and hydrological properties on the level of material damage and stress. During loading (injection), the rock is damaged and its mechanical properties change by many orders of magnitude. For example, when failure is in tension, the stiffness of the rock that is usually several GPa, vanishes just before failure (Lockner and Byerlee, 1980; Lockner et al., 1992). The ability to account for these large changes of many orders of magnitude in rock properties is essential for reliable modeling. The nucleation and propagation of faults induced by wellbore fluid injection was studied by Shalev and Lyakhovsky (2013).

The goal of this paper is to present the formulation and implementation of our novel numerical software called *Hydro-PED* that simulates the coupled multi-processes that occur during hydraulic stimulation. Results of three dimensional simulations illustrate the importance of modeling in studying the physical processes associated with hydraulic stimulation.

FORMULATION

Following Kachanov (1986), we use Continuum Damage Mechanics (CDM), on which the damage variable represents the local crack density and is related to the reduction of the rigidity of a spatial domain relative to the modulus of an ideal fracture free solid. The non-linear visco-elastic damage rheology model of Lyakhovsky et al. (1997) and Hamiel et al. (2004a,b) provides a framework for simulating fracturing and faulting processes at various scales. This model accounts for the following

general aspects of brittle rock deformation: (1) Non-linear elasticity that connects the effective elastic moduli to a damage variable and loading conditions; (2) Evolution of the damage state variable as a function of the ongoing deformation and gradual conversion of elastic strain to permanent inelastic deformation during material degradation; (3) Macroscopic brittle instability at a critical level of damage and related rapid conversion of elastic strain to permanent inelastic strain; (4) Coupling between deformation and porous fluid flow through poroelastic constitutive relationships incorporating damage rheology with Biot's poroelasticity. This formulation is distinctive in the way it accounts for the dependency of the mechanical and hydrological properties on damage, and in the formulation of the shear-related dilatancy.

Solid Deformation

The two governing equations are solid force equilibrium and fluid mass conservation. The force equilibrium is given by:

$$\sigma_{ij,j} + f_i = 0 \qquad (1)$$

where σ_{ij} is the stress tensor and f_i is the body force vector. The poroelastic constitutive relationship between the stress and strain incorporating damage rheology with Biot's poroelasticity (e.g., Hamiel et al., 2004a) is written as

$$\sigma_{ij} = \left(\lambda I_1 - \gamma\sqrt{I_2}\right)\delta_{ij} + \left(2\mu - \gamma\frac{I_1}{\sqrt{I_2}}\right)\varepsilon_{ij} - \alpha_B p\delta_{ij} \qquad (2)$$

where $I_1 = \varepsilon_{kk}$ and $I_2 = \varepsilon_{ij}\varepsilon_{ij}$ are the first and second invariants of the elastic strain tensor ε_{ij}, λ and μ are the Lamé parameters of linear Hookean elasticity, γ is a third modulus for a damaged solid, α_B is Biot constant, and p is the pore pressure. In equation 2 the three terms on the right hand side represent the volumetric strain, shear strain, and poroelastic effect, respectively. The coupling between the volumetric and shear strain is introduced by the shear term ($-\gamma\sqrt{I_2}$) in the volumetric component and a volumetric term ($-\gamma I_1/\sqrt{I_2}$) in the shear component. This coupling is responsible for nonlinear elastic dilation of the rocks during shearing as shown in laboratory experiments (e.g. Lockner and Byerlee, 1994).). This formulation provides a consistent solution for coupling of shear stress and pore pressure changes under undrained conditions observed by Lockner and Stanchits (2002) and modeled by Hamiel et al. (2005).

Below the onset of damage (γ=0), equation 2 reduces to the Hookean linear elastic formulation. With the onset of damage accumulation, the effective elastic moduli change proportionally to the evolving damage state variable $0 \le \alpha_D \le 1$. The transition from damage accumulation to healing is controlled by the value of the strain invariants ratio $\xi = I_1/\sqrt{I_2}$ which is connected to the internal friction angle of Byerlee's law (Byerlee, 1978). The rate of damage/healing accumulation is given by (Lyakhovsky et al., 1997):

$$\frac{d\alpha_D}{dt} = \begin{cases} C_d I_2(\xi - \xi_0) & for \quad \xi > \xi_0 \\ C_1 \exp\left(\frac{\alpha_D}{C_2}\right) I_2(\xi - \xi_0) & for \quad \xi < \xi_0 \end{cases} \qquad (3)$$

where the coefficient C_d is the rate of positive damage evolution (material degradation) and is constrained by laboratory experiments (Lyakhovsky et al., 1997; Hamiel et al., 2004b; 2009). The rate of damage recovery (material healing) is assumed to depend exponentially on α_D. This produces logarithmic healing with time in agreement with the behavior observed in laboratory experiments (e.g., Dieterich and Kilgore, 1996; Scholz, 2002; Johnson and Jia, 2005) with rocks and other materials. Lyakhovsky et al. (2005) showed that the damage model with exponential healing (equation 3) reproduces the main observed features of rate- and state-dependent friction and constrained the coefficients C_1, C_2 by comparing model calculations with laboratory frictional data. The evolving damage state variable α_D is calculated by the integration of $d\alpha_D/dt$ in time. We assume that the elastic moduli depend linearly on damage (Agnon and Lyakhovsky, 1995):

$$\begin{aligned} \lambda &= const. \\ \mu &= \mu_0 + \gamma_r \xi_0 \alpha_D \\ \gamma &= \gamma_r \alpha_D \end{aligned} \qquad (4)$$

where μ_0 is the initial shear modulus of the intact rock and γ_r is a scaling constant that gives the values of the moduli at maximum damage level (α_D=1).

Seismic Events

When deformation achieves a threshold state ($\xi=\xi_0$), damage increases, weakening the material element. Damage increase leads to decreasing shear modulus, increasing Poisson ratio, and amplification of the nonlinearity of the effective rock elasticity (equation 4). The damage increase toward its critical level leads to brittle instability and a macroscopic event in one of two modes of failure, tensile and shear failure (Lyakhovsky et al., 1997; Lyakhovsky and Ben-Zion, 2008). The onset of the brittle instability is triggered by the loss of convexity of the elastic strain energy function, which is mathematically expressed by two

conditions (equation 14 and 15 of Lyakhovsky et al., 1997). One condition is realized under moderate damage values and high values of the strain invariants ratio corresponding to tensile stresses. The second condition is realized at higher damage values, but under more compressive loading (see Fig. 1 from Lyakhovsky et al., 1997). In the first case the mode-I macroscopic failure leads to complete stress drop keeping fluid pressure inside a failed element (hydro-fracturing). This periodically occurs within already developed fracture that has very low stiffness in the damaged rock. As a result, the stress is also low within the fracture and the pore pressure may exceed the least principal stress. The second mode-II failure condition is modeled by assuming the existence of slipping surfaces within the failed elements, equivalent to a planar fault along which the failing material undergoes frictional sliding (hydro-shearing). Lyakhovsky and Ben-Zion (2008) developed a mathematical procedure for the local stress drop that produces a rapid release of the elastic energy and accumulation of a permanent plastic strain. They utilize the Drucker-Prager model, which generalizes the classical Coulomb yield condition for cohesion-less material. They use scaling relations between the rupture area and seismic potency values established in the seismology and typical range of the stress drop (1-10 MPa) during earthquakes, to calibrate parameters of their local stress drop procedure and connect them to the dynamic friction (~0.2) of simpler models with planar faults.

Simulations with the discussed model produce quasi-dynamic stress drops and scaling relations between rupture areas and seismic potency values that are consistent with classical theoretical results and observations summarized by Kanamori and Anderson (1975). Following the mode-II event, the slip associated with the macroscopic brittle failure is arrested and post-failure material healing starts.

Groundwater Flow

The fluid mass conservation equation for saturated isothermal flow is (e.g., Wang, 2000):

$$\nabla \cdot \left(\frac{\underline{\boldsymbol{k}}(\alpha_D)}{\mu_f} (\nabla p + \rho g \mathbf{z}) \right) = S_\varepsilon \frac{\partial p}{\partial t} + \alpha_B \frac{\partial \varepsilon_{kk}}{\partial t} \qquad (5)$$

where $\underline{\boldsymbol{k}}$ is the intrinsic permeability of the medium, μ_f is the fluid viscosity, ρ is the fluid density, g is the gravitational acceleration, z is a unit vector, and S_ε is the specific storage at constant strain. We assume that the permeability depends exponentially on damage (e.g., Picandet et al., 2001):

$$\underline{\boldsymbol{k}}(\alpha_D) = \underline{\boldsymbol{k}}_o * exp(b\alpha_D) \qquad (6)$$

where $\underline{\boldsymbol{k}}_o$ is the initial permeability tensor and b is a constant.

NUMERICAL IMPLEMENTATION

The implementation of the above formulation into the numerical code *Hydro-PED* uses two numerical methods: Finite Element Method (FEM) and Explicit Finite Difference Lagrangian Method (EFDLM). Solid deformation is solved with EFDLM and fluid mass conservation is solved using FEM. Fluid pressure solved by the fluid mass conservation equation is used in the solid deformation procedure as a known parameter and the displacements calculated by the solid deformation equations are used the fluid mass conservation procedure as known parameters. The numerical algorithm is coded using Fortran 90 and Open Multiprocessing programming on IBM power 7 workstations running the AIX Unix operating system.

Solid Deformation Implementation

Explicit Finite Difference Lagrangian Method (EFDLM) fully explicit numerical method relies on a large-strain explicit Lagrangian formulation originally developed by Cundall (1989). The formulation is explicit-in-time, using an updated Lagrangian scheme to provide the capability for large strains. This algorithm offers advantages over conventional finite element schemes in case where material instability occurs. The general procedure involves solving a force balance equation for each grid point in the body:

$$\frac{\partial v_i}{\partial t} = \frac{F_i}{m} \qquad (7)$$

where v_i and F_i are velocity and force applied to a node of mass m. Solution of the equations of motion provides velocities at each grid point, which are used to calculate element strains. These strains being substituted into the linear or non-linear constitutive relation provide element stresses and then forces acting at the element faces. These forces recalculated to the grid nodes are the necessary input for the solution of the equation of motion on the next step of calculation cycle.

The computational mesh consists of 4-points tetrahedral elements. Four linear element shape function L_k ($k=1,4$ – number of element node) are

$$L_k = a_k + b_k x_1 + c_k x_2 + d_k x_3 \qquad (8)$$

where a_k, b_k, c_k, d_k are constants and (x_1, x_2, x_3) are coordinates inside the element. These shape functions are used to linearly interpolate the nodal velocities ($V_i^{(k)}$) within each element and enables the calculation of the strain increments $\Delta\varepsilon_{ij}$

$$\Delta\varepsilon_{ij} = \Delta t \cdot \sum_{k=1}^{4} \left(V_i^{(k)} \frac{\partial L_k}{\partial x_j} + V_j^{(k)} \frac{\partial L_k}{\partial x_i} \right) \qquad (9)$$

While elastic strains are calculated the stress tensor is computed using constitutive relation (equation 2), which includes fluid pressure and local damage-

dependent values of the elastic moduli in the specific element (equation 4). The nodal forces are then a vector sum of one third of forces acting on all triangle faces of the tetrahedral elements adjacent to the node:

$$F_i = \sum_{faces} \frac{1}{3} \sigma_{ij} n_j + m g_i \qquad (10)$$

where n_j is a normal vector to the face, node mass m is one third of the mass of elements adjacent to the node, and g_i – gravity acceleration vector. Once the forces are known, new velocities are computed by integrating (equation 7) over a given time step.

$$V_i^{(n)}(t+\Delta t) = V_i^{(n)}(t) + \left[F_i^{(n)} - \chi \left|F_i^{(n)}\right| sign\left(V_i^{(n)}\right)\right] \frac{\Delta t}{m_{inert}} \qquad (11)$$

where χ is a damping parameter and m_{inert} is a density scale factor. During the integration, the previously calculated force ($F_i^{(n)}$) is damped. The damping term $0<\chi<1$ is proportional to the acceleration (out-of-balance) force and sign opposite to velocity, dissipate energy of the system and attenuate elastic waves traveling in the simulated area. This term vanishes if the system is in equilibrium and provides a convergence of numerical procedure to a steady-state solution. Following Poliakov et al. (1993) we use "inertial" mass in equation 11 instead of "gravity" mass in equation 7 to allow adaptive time scaling. The time step, which provides stability of the numerical scheme, is:

$$\Delta t = \frac{1}{2} \frac{\Delta x}{V_p} \qquad (12)$$

where Δx is a minimal distance between grid points and V_p is maximum possible seismic velocity in the material. Introducing density scale factor ($m_{inert}=D_s$ m) we decrease V_p as square root of D_s and proportionally increase the time step without any numerical artifacts. This could be done only if the system is close to equilibrium (out-of-balance force approaches to zero). This adaptive procedure, starting with $D_s=1$, automatically increases D_s if the system is in a steady-state regime, or brings it back to "1", if the solution deviates from static.

The damage level (α_D) for each element is calculated for every numerical cycle according to equation 3 with time step defined by the adaptive procedure. If damage in one element achieves its critical level, the stress drop occurs and plastic strain is accumulated in this specific element. The stress recalculation repeats until full equilibration is reached. This stress drop may trigger failure in other elements where the stress drop procedure is activated. Finally, the list of elements involved in the failure process and accumulated plastic strain components are recorded together with the values of the stress drop for calculation of the potency and moment of the seismic event.

Because in this EFDLM implementation the equations are solved locally without establishment of a global stiffness matrix, elements that have no stiffness (after tension failure) could be eliminated. The ability to account for these features is essential for hydraulic stimulation modeling because, as damage develops, the stiffness of the rock (element) changes from its original values of E =4,000 MPa when there is no damage to a few MPa when α_D=1, or even to zero when failure is in tension. These features are hard to incorporate in FEM where they cause numerical instabilities. To avoid these instabilities, many FEM codes relate the elastic parameters to strain or artificially limit the range of damage change preventing element failure. As opposed to the force equilibrium equation with damage, the diffusion equation of the fluid mass conservation is very stable in FEM, and we use it in our formulation.

Fluid Mass Conservation

The fluid mass conservation is implemented using the finite element method developed in this study closely follows the formulation of Lewis and Schrefler (1987).

$$(\boldsymbol{S} + \Theta \boldsymbol{H} \Delta t) p_{n+1} = \boldsymbol{L}^T \Delta u + [\boldsymbol{S} - (1-\Theta)\boldsymbol{H}\Delta t] p_n + \boldsymbol{F}\Delta t \qquad (13)$$

where $0 \le \Theta \le 1$ is the time stepping weight coefficient and Du is the incremental displacement. The arrays of equation 13 are defined as:

$$\boldsymbol{S} = \int_\Omega N^T S_\varepsilon N d\Omega \qquad (14a)$$

$$\boldsymbol{H} = \int_\Omega B^T \frac{\boldsymbol{k}}{\mu} B d\Omega \qquad (14b)$$

$$\boldsymbol{L}^T = \int_\Omega N^T \alpha_B B d\Omega \qquad (14c)$$

$$\boldsymbol{F} = -\int_\Gamma N^T q d\Gamma - \int_\Omega B^T \frac{k}{\mu} B \rho g \nabla z d\Omega \qquad (14d)$$

where N and N^T are the same linear shape functions as in equation 8 and their transposed vectors, respectively, and B and B^T are the shape functions gradients and their transposed vectors, respectively. q is a fluid source term. We note that in this formulation, the displacements are calculated separately and are known a priory and are therefore written on the right hand side. The first term on the right hand side of equation 13 represent the poroelastic effect of the strain. We use the 3D grid with the same tetrahedral elements as in the EFDLM implementation, eliminating any interpolations during variable transfer between FEM and EFDLM.

Because displacements can be significant, shape functions are calculated on every time step. Permeability is also updated on every time step by equation 6. Once the fluid stiffness matrix and the fluid load vectors are formed, the system of equations is solved with the parallel HSL solver (HSL, 2011).

RESULTS

In this section we show an example of injection into a well within a cylinder domain with a radius of 40m that contains 76,718 tetrahedral elements. Fluid is injected at the center of the domain into a well with radius of 50cm. Elements length varies from 5cm around the injection well to 4m at the outer boundary. The principal stresses are assigned as:

$$\sigma_V = \rho_S g z - \alpha_B p \quad (15a)$$

$$\sigma_{H\,max} = 2\sigma_v \quad (15b)$$

$$\sigma_{h\,min} = 0.5\sigma_v \quad (15c)$$

$$p = \rho_f g z \quad (15c)$$

where ρ_s=2600kg/m^3 and ρ_f=1000kg/m^3. The nodes that define the well are assigned with force boundary conditions that are equal to the fluid pressure in the well, whereas the outer boundary has fixed zero displacement conditions. Fluid outer boundary conditions are zero flux. The fluid pressure at the well is assign to be 50 MPa above hydrostatic. Initial and boundary conditions along with mechanical and hydrological parameters are listed in table 1. Mechanical and hydrological parameter values represent values of granite (Wang, 2000). Initially, the domain is assumed to be homogeneous. Heterogeneous evolutions of the mechanical and hydrological parameters occur as a response to injection. In nature, domains are never homogeneous. Faults and fractures exist to some extent in all sites. This heterogeneity may control initiation and progression of micro-seismic activity. The goal of this study is to understand the physical behavior of the simplest domain. The effect of initial heterogeneity will be examined in future work.

The damage shown in Figure 1 propagates away from the injection well in the center of the circle and creates two faults in an angle of 17.5^0 of the principal axis.

The pore pressure (Fig. 2) increases mainly within the damaged rock where the enhanced reservoir is created and permeability is high. The only minor pore pressure changes occurring in the undamaged rock result from poro-elastic effects of the advancing faults. Each element within the damage zone undergoes many sequential loops of damage accumulation, stress drop, and healing, resulting with an average damage value within the reservoir o about 0.7 (Fig. 1). In this simulation we set a maximum possible permeability of 10^{-13} m^2 (five orders of magnitude higher than the undamaged rock). Hence, the permeability is 10^{-13} m^2, whenever damage is greater than 0.7 (equation 6 and table 1). With this high permeability, pore pressure within the damaged zone is efficiently being transferred from the injection well to the tips of the damaged zones.

Table 1: parameters used in the simulations

k_0 (eq. 6)	10^{-19} m^2
a (eq. 6)	20
E	4000 MPa
ν	0.3
ξ_0 (eq. 3,4)	-0.8
γ_r (eq. 4)	920 MPa
C_d (eq. 3)	*10*
C_1 (eq. 3)	*10^{-8}*
C_2 (eq. 3)	0.03
α_B (eq. 2,5)	1
Sε (eq. 5)	5*10^{-11}1/Pa

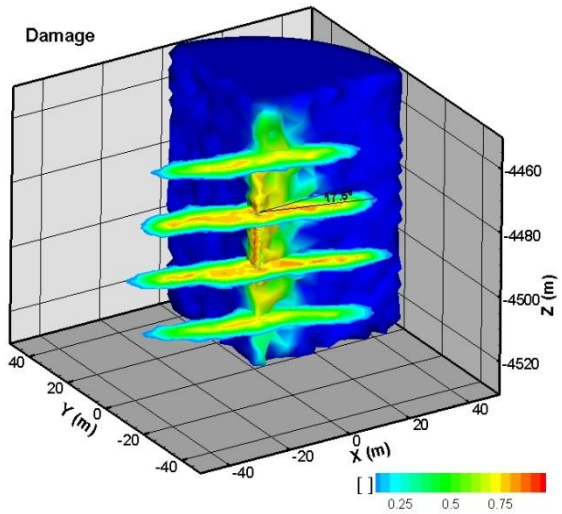

Figure 1: Damage after 80 hours of injection

Both the mean stress (Fig. 3) and the shear stress, J_2, expressed as the second invariant of the stress tensor (Fig. 4) show stress concentration affected by the damaged zones tips. Within the damage zone, stresses are low. The occurrence of low stress and high pore pressure within the damage zone promote tensile failure (hydro-fractures).

The distance of the seismicity from the injection well over time is shown in Figure 5. This seismicity represents the growth rate of the enhanced reservoir. Seismicity starts after about four hours of injection and occurs continuously along the entire damaged zone. Fault propagation accelerates for 30 hours and then remains at a constant pace until the end of the simulation. These velocities are relatively slow compared to data of field stimulation because flow rates here are also much smaller. The velocity

depends on the supply of fluid pressure from the injection well to the tip of the propagating enhanced reservoir. This supply depends on the permeability and length of the reservoir. High permeability transfers the pressure fast. At some point (> 30 hours), the reservoir grows to be too long to maintain high pore pressure at its tip and acceleration decreases.

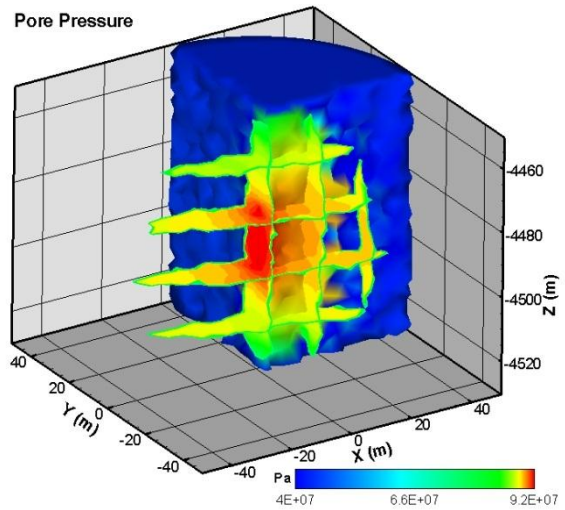

Figure 2: Pore pressure after 80 hours of injection. The contour level distribution is not linear to allow the large values differences between the damaged zone interior and exterior.

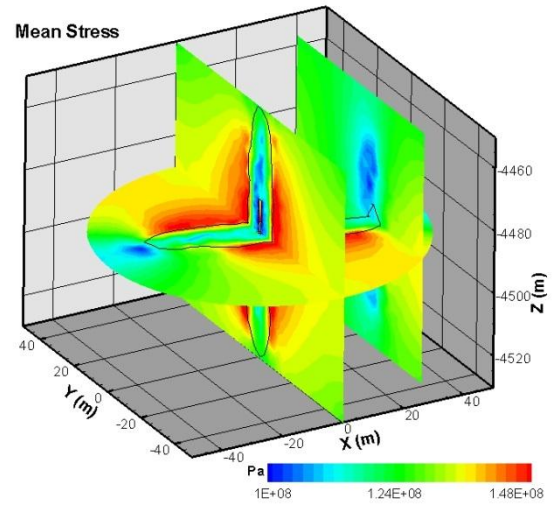

Figure 3: Mean Stress after 80 hours of injection

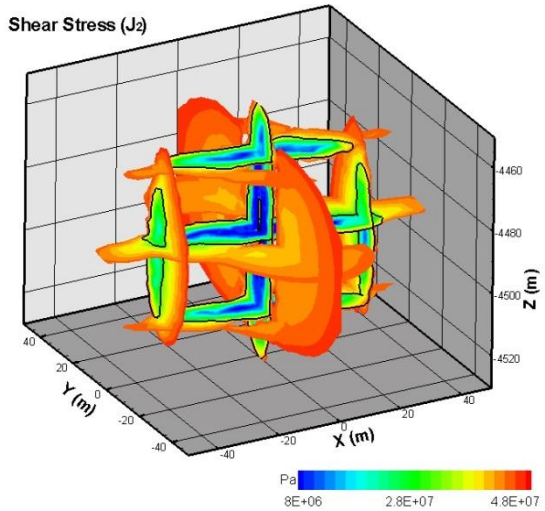

Figure 4: Shear Stress shown as the second invariant of the stress tensor (J_2), after 80 hours of injection.

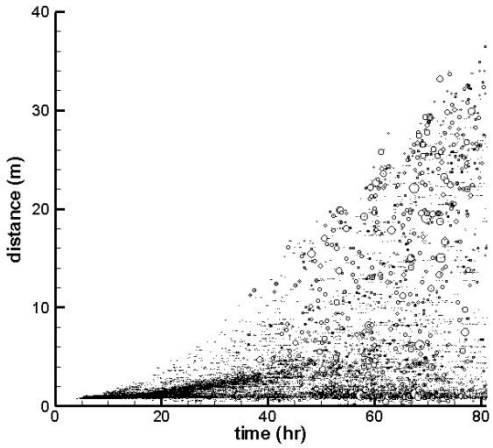

Figure 5: The distance of seismicity from the injection well over time.

CONCLUSION

The novel code *Hydro-PED* is shown to provide results similar to field hydraulic stimulations. *Hydro-PED* uses the Explicit Finite Difference Lagrangian Method to solve the solid deformation equations and the Finite Element Method for solving fluid mass conservation. Rock properties are coupled with the state of damage and seismic events are nucleated as damage grows to a value (~1) that causes the loss of convexity of the elastic strain energy function. The seismic event is simulated by stress drop that produces a rapid release of the elastic energy and accumulation of a permanent plastic strain (Drucker-Prager model).

Results show that the propagation of the enhanced damaged reservoirs could be divided into three stages which duration depends on the tectonic stresses, injection pressure and material properties. The duration of the first stage of fluids flow into the rock with no seismic events is four hours under the conditions specified in this study. The duration of the second stage from the onset of seismic events till the end of accelerated seismic activity is 30 hours. Pore pressure at the tip of the reservoirs is above 90% of the pressure in the injection well. The velocity of the advancing reservoirs is limited only by the rate of damage accumulation. The third stage with decelerated reservoir growth lasts until the end of injection; it was simulated during >30 hours. Fluid transport becomes a limiting factor as the reservoirs are too long to efficiently transfer the pressure from the well to the reservoir tip.

REFERENCES

Adachi, J., Siebrits, E., Peirce, A., and Desroches, J. (2007), "Computer simulation of hydraulic fractures", *Int. J. Rock Mech. Min. Sci.*, **44,** 739–757.

Agnon, A. and Lyakhovsky, V. (1995), "Damage distribution and localization during dyke intrusion", in *The Physics and Chemistry of Dykes*, pp. 65–78, eds Baer, G. and Heimann, A., Balkema, Rotterdam.

Baisch, S., Vörös, R., Rothert, E., Stang, H., Jung, R., and Schellschmidt, R. (2010), "A numerical model for fluid injection induced seismicity at Soultz-sous-Forêts", *Int. J. Rock. Mech. Min. Sci.*, **47**, 405–413.

Byerlee, J.D. (1978), "Friction of rocks", *Pure Appl. Geophys*., **116**, 615–626, doi:10.1007/BF00876528.

Cuenot, N., Dorbath, C., and Dorbath, L. (2008), "Analysis of the microseismicity induced by fluid injections at the Hot Dry Rock site of Soultz-sous-Forets (Alsace, France): implications for the characterization of the geothermal reservoir properties," *Pure Appl. Geophys*., **165**, 797–828.

Cundall, P.A., (1989), "Numerical experiments on localization in frictional materials", *Ign. Arch*., **59**, 148-159.

Dieterich, J.H., and Kilgore, B.D. (1996), " Imaging surface contacts; power law contact distributions and contact stresses in quarts, calcite, glass, and acrylic plastic", *Tectonophysics*, **256**, 219–239, doi:10.1016/0040-1951(95)00165-4.

Fischer, T., Hainzl, S., Eisner, L., Shapiro, S.A., and Le Calvez, J. (2008), " Microseismic signatures of hydraulic fracture growth in sediment formations: Observations and modeling", *J. Geophys. Res.*, **113**, B02307, doi:10.1029/2007JB005070.

Hamiel, Y., Lyakhovsky, V., and Agnon, A. (2004a), "Coupled evolution of damage and porosity in poroelastic media: theory and applications to deformation of porous rocks", *Geophys. J. Int*., **156**, 701-713.

Hamiel, Y., Liu, Y., Lyakhovsky, V., Ben-Zion, Y. and Lockner, D. (2004b), "A visco-elastic damage model with applications to stable and unstable fracturing", *J. Geophys. Int.*, **159**, 1-11.

Hamiel, Y., Lyakhovsky, V., and Agnon, A. (2005), "Rock dilation, nonlinear deformation, and pore pressure change under shear", *Earth Planet. Sci. Lett*., **237**, 577–589, doi:10.1016/j.epsl.2005.06.028.

Hamiel, Y., Lyakhovsky, V., Stanchits, S., Dresen, G., and Ben-Zion, Y. (2009), "Brittle deformation and damage-induced seismic wave anisotropy in rocks", *Geophys. J. Int.*, **178**, 901-909.

Hossain, M.M. and Rahman, M.K. (2008), "Numerical simulation of complex fracture growth during tight reservoir stimulation by hydraulic fracturing", *J. Pet. Sci. Eng.*, **60**, 86–104.

HSL (2011), A collection of Fortran codes for large scale scientific computation. http://www.hsl.rl.ac.uk

Johnson, P.A., and Jia, X. (2005), "Non-linear dynamics, granular media and dynamic earthquake triggering", *Nature*, **437**, 871–874, doi:10.1038/nature04015.

Kachanov, L.M. (1986), *Introduction to Continuum Damage Mechanics*, 135 pp., Martinus Nijhoff, Dordrecht, Netherlands.

Kanamori, H. and Anderson, D.L. (1975), "Theoretical basis of some empirical relations in seismology", *Bull. seism.. Soc. Am.*, **65,** 1073–1095.

Kohl, T., and Megel, T. (2007), "Predictive modeling of reservoir response to hydraulic stimulations at the European EGS site Soultz-sous-Fôrets", *Int. J. Rock. Mech. Min. Sci.*, **44**, 1118-1131.

Lee, S.H., and Ghassemi, A. (2011), "Three dimensional Thermo-Poro-Mechanical Modeling of Reservoir Stimulation and Induced Microseismicity in Geothermal Reservoir",

Thirty Sixth Workshop on Geothermal Reservoir Engineering, Stanford University, Stanford,California, SGP-TR-191.

Lewis, R.W., and Schrefler, B.A. (1987), *The Finite Element Method in the Deformation and Consolidation of Porous Media*, John Wiley and Sons, New York.

Lockner, D.A. and Byerlee, J.D. (1980), "Development of fracture planes during creep in granite", in 2nd conference on acoustic emission/microseismic activity in geological structures and materials, pp. 11–25, eds Hardy, H.R. and Leighton, F.W., Trans-Tech. Publications, Clausthal-Zellerfeld, Germany.

Lockner, D.A., Byerlee, J.D., Kuksenko, V., Ponomarev, A. and Sidorin, A. (1992), "Observations of quasi-static fault growth from acoustic emissions. in Fault mechanics and transport properties of rocks", *International Geophysics Series*, **51,** pp. 3–31, eds Evans, B. and Wong, T.-f., Academic Press, San Diego, California.

Lockner, D.A., and Byerlee, J.D. (1994), "Dilatancy in hydraulically isolated faults and the suppression of instability", *Geophys. Res. Lett*., 21, 2353-2356.

Lockner, D.A. and Stanchits, S.A. (2002), "Undrained poroelastic response of sandstones to deviatoric stress change", *J. Geophys. Res*. **107**, doi: 10.1029/2001JB001460.

Lyakhovsky, V., Ben-Zion, Y., and Agnon, A. (1997), "Distributed damage, faulting, and friction", *J. Geophys. Res*., **102**, 27,635–27,649.

Lyakhovsky, V., Ben-Zion, Y. and Agnon, A. (2005), "A viscoelastic damage rheology and rate- and state-dependent friction", *Geophys. J. Int.*, **161**, 179–190.

Lyakhovsky, V., and Ben-Zion, Y. (2008), "Scaling relations of earthquakes and aseismic deformation in a damage rheology model", *Geophys. J. Int.*, **172**, 651-662.

Pearson, C. (1981), "The relationship between microseismicity and high pore pressures during hydraulic stimulation experiments in low permeability granitic rocks", *J. Geophys. Res.*, **86**, 7855–7864.

Picandet, V., Khelidj, A., and Bastian, G. (2001), "Effect of axial compressive damage on gas permeability of ordinary and high performance concrete", *Cement. Concrete Res.*, **3**, 1525–1532.

Poliakov, A., Cundall, P., Podladchikov Y., and Lyakhovsky V. (1993), "An explicit inertial method for the simulation of viscoelastic flow: an evaluation of elastic effects on diapiric flow in two- and three-layers model", In: Runcorn, K.E., Stone, D. (Eds.), *Dynamic Modeling and Flow in the Earth and Planets*, Proceedings of the NATO Advanced Study Institute, Kluwer, Dordrecht, 175-195.

Scholz, C.H. (2002), *The Mechanics of Earthquakes and Faulting*, 2nd ed., 471 pp.

Shalev, E., and Lyakhovsky, V. (2013), "The processes controlling fault propagation induced by wellbore fluid injection," submitted to *Geophys. J. Int.,*

Šílený, J., Hill, D.P., Eisner, L., and Cornet, F.H. (2009), "Non–double-couple mechanisms of microearthquakes induced by hydraulic fracturing", *J. Geophys. Res.*, **114**, B08307, doi:10.1029/2008JB005987.

Tang, C.A., Tham, L.G., Lee, P.K.K., Yang, T.H., and Li, L.C. (2002), "Coupled analysis of flow, stress and damage (FSD) in rock failure", *Int. J. Rock Mech. Min. Sci.*, **39**, 477–89.

Wang, H.F. (2000), *Theory of Linear Poroelasticity with Applications to Geomechanics and Hydrogeology*, Princeton University Press.

Wang, S.Y., Sun, L., Au, A.S.K., Yang, T.H., and Tang, C.A. (2009), "2D-numerical analysis of hydraulic fracturing in heterogeneous geo-materials", *Constr. Build Mater.* **23**, 2196–2206.

Zhao, X., and Young, R.P. (2011), "Numerical modeling of seismicity induced by fluid injection in naturally fractured reservoirs", *Geophysics*, **76**, WC167.

Zoback, M., and Harjes, H.-P. (1997), "Injection-induced earthquakes and crustal stress at 9 km depth at the KTB deep drilling site, Germany," *J. Geophys. Res.*, **102**, 18,477–18,491.